Multi-modal Circuit Model Derivation for Finite Thickness Frequency Selective Surfaces

Ahmed D. Alwakil, Ronan Sauleau, Mauro Ettorre

Multi-modal Circuit Model Derivation for Finite Thickness Frequency Selective Surfaces

Ahmed D. Alwakil, Ronan Sauleau, *Fellow, IEEE* and Mauro Ettorre, *Fellow, IEEE*

***Abstract*—We propose a simplified approach to compute the multi-modal equivalent circuit model of a Frequency Selective Surface (FSS) with periodic unit cells, under normal plane wave incidence. Floquet's periodic boundary conditions are replaced by perfect electric and magnetic boundaries arranged according to the incident field polarization. The electromagnetic scattering from the FSS is modeled as a generalized rectangular waveguide (GRW) discontinuity problem. The Generalized Transverse Resonance technique is proposed to analyze the FSS unit cell aperture which is modeled as a waveguide of a finite thickness. The cutoff frequencies and the cross-sectional profile of the FSS waveguide modes are found. Projection matrices are then computed between the FSS's GRW modes and the GRW modes outside the FSS, leading to the full modal network. The proposed method is validated by full-wave numerical results for finite-thickness patch-based FSS.**

***Index Terms*—Circuit models, mode matching methods, Frequency Selective Surfaces, Transverse resonance method.**

I. Introduction

The derivation of circuit models (CM) to quantify the electromagnetic scattering from frequency selective surfaces (FSS) [1] due to plane wave illumination, had received recent interest due to its role in designing various RF components such as polarizers [2]. Scattering of normally incident plane waves over an FSS with periodic unit cells in a rectangular lattice presents the same behavior of reflection and transmission of a waveguide discontinuity in a generalized rectangular waveguide (GRW) [3]. The similarity stems from replacing the Floquet boundary conditions surrounding the FSS unit cell with two opposite perfect electric conductors (PEC) walls, and two perfect magnetic conductors (PMC) walls [4]. In this analogy, the incident plane wave corresponds to the fundamental mode of the incident GRW, and the FSS unit cell is modeled as a subsequent GRW with the discontinuous interface causing scattering. Following this approach, the transverse fields over the FSS aperture are required to compute the equivalent CM of the unit cell. Different approaches had been proposed to evaluate the aperture fields, either by using full-wave simulations for geometrically complex structures [5], [6], or by approximating the fields by piece-wise analytical functions for simpler geometries [6]. With respect to the analytical approach, transverse fields at the aperture are assumed to be separable into frequency and spatial terms with the latter not varying within the band of interest. This assumption is limited to electrically thin FSS neglecting the propagation effects along the FSS thickness and its usage is valid below the second resonance of the FSS aperture [7], [8] as well as to sparsely distant cascaded FSSs where aperture fields are not strongly coupled [9].

On the other hand, the generalized transverse resonance (GTR) method [10], which is a multimodal generalization of transverse equivalent networks [11], [12], computes for the resonant modes for arbitrarily shaped all-metal waveguides [13]. The resonance of each waveguide mode is found by considering the propagation of the corresponding longitudinal magnetic and electric section submodes [14] in the waveguide cross-sectional plane. After applying boundary conditions at the edges, a characteristic matrix is found at any line cutting the waveguide cross-section and is normal to the propagation of the submodes. This characteristic matrix is the summation of right and left (to the line) multi-modal input admittances. The main difficulty with GTR usage stems from deriving the cutoff frequencies of the waveguide modes, which is done by searching for the zeros for a characteristic matrix determinant [15], or the singular value due to singular value decomposition of the same characteristic matrix [16]. Both approaches suffer from numerical instabilities for large characteristic matrices.

In this paper, we show that under normal incidence, the aperture field of a thick FSS unit cell GRW is computed using the GTR method, where the field is found as a sum of GRW waveguide modes. Also, we propose a simplifying modification over GTR for determining the FSS-GRW cutoff frequencies, by searching for frequencies at which an input scalar admittance vanishes. Afterward, the admittance matrix of the FSS multi-modal network is found [17], [18] which can be reduced into a two-port lumped network [19] when the input and output GRWs are monomodal. The proposed method is explained using patch FSS [20]–[22] as a case study, and the model is verified by full-wave simulation. This method was adopted for aperture-based FSS with arbitrary thickness, including thin FSSs [23], and could be adapted for arbitrary unit cell shapes as long as the aperture can be converted into rectangular blocks using staircase approximations, including simple geometries [24]. Finally, this method provides an exact analytical derivation of the FSS aperture field in a systemic way for a single or cascaded FSSs with no validity constraints.

II. GTR Formulation

Fig. 1(a) shows the case study of the patch-based FSS with periodicity P_x and P_y along $x-$ and $y-$axes respectively. For simplicity, the metallic patches are assumed to be PEC and immersed within a media of permittivity ϵ_B with $2d_B$ thickness. It is assumed that the incident plane wave is Y-

This work was supported by Centre National d'Études Spatiales (CNES) under the R&T activity R-S18/TC-0006-019. A. D. Alwakil, R. Sauleau, M. Ettorre are with Univ. Rennes, IETR (Institut d'Electronique et des Technologies du numéRique) - UMR 6164, CNRS, 35000 Rennes, France (ahmed.alwakil@univ-rennes1.fr).

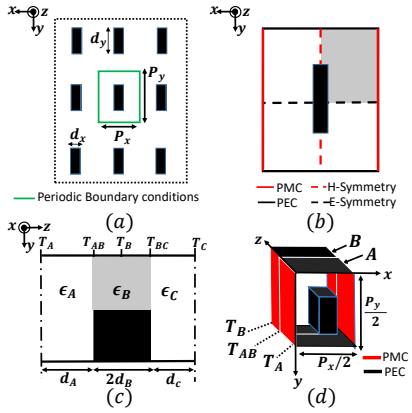

Fig. 1. (a) Geometry of the patch-based FSS. (b) Top view of the unit cell and in grey the primitive unit cell. (c) Cross-section projectional view of the primitive unit cell and its surroundings with the top and lower boundaries as PEC. (d) 3D schematic of the GRW discontinuity junction with the input and output terminals defined at the reference planes T_A and T_B.

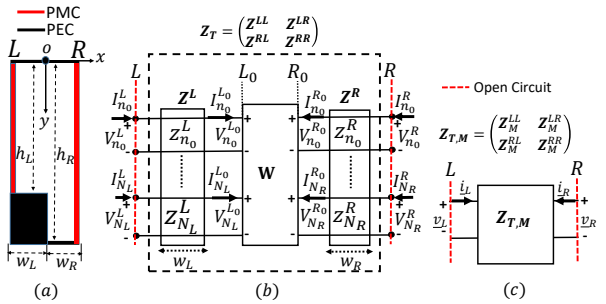

Fig. 2. (a) Schematic of the FSS-GRW waveguide cross-section with the dimensions $w_L = \frac{d_x}{2}$, $w_R = \frac{P_x - d_x}{2}$, $h_L = \frac{P_y - d_y}{2}$ and $h_R = \frac{P_y}{2}$. (b) Corresponding GTR multi-modal network representation. (c) GTR network representation at the resonance frequency $f = f_M$.

polarized, accordingly, Floquet boundary conditions are replaced by PEC and PMC walls as shown in Fig. 1(b). Also, Fig. 1(b) shows the reduced FSS-GRW unit cell (grey colored) where the mirror symmetry planes are replaced by PEC (for E- symmetry) and PMC (for H- symmetry) walls respectively. The FSS is surrounded by two GRWs filled with media ϵ_A and ϵ_C as shown in Fig. 1(c). Also, Fig. 1(d) shows the 3D view of the GRW discontinuity between planes T_A and T_B.

The next step is to apply the GTR method to the FSS-GRW cross-section shown in Fig. 2(a). It is required to compute cutoff frequencies and the profile distributions for the transverse electric (TE_z) (i.e. $E_z = 0$) and transverse magnetic (TM_z) (i.e. $H_z = 0$) modes. On the other hand, the transverse electric magnetic (TEM_z) (i.e. $E_z = H_z = 0$) mode has a zero cutoff frequency and its profile distribution is found by solving Laplace's equation [25] which is outside the scope of GTR and will not be discussed in this paper.

a) GTR for TE_z and TM_z modes : From the GTR perspective, the resonance of a GRW waveguide mode (i.e. at its cutoff frequency) is due to the propagation of the transverse (with respect to the x-axis) TE_x ($E_x = 0$) or TM_x ($H_x = 0$) sub-modes along the x-axis [13]. These transverse sub-modes are parallel plate waveguide (PPW) modes. Fig.2(b) shows the multimodal network of the sub-modes, where the FSS-GRW cross-section is modeled as a 2D cavity of two x-aligned PPW-modal transmission lines, connected by a step junction and terminated by PMC walls on both sides. Since the FSS-GRW cross-section is of uniform medium, the FSS resonant TM_z/TE_z modes are independent and each mode has its own GTR multi-modal network due to the transverse propagation of the PPW TE_x/TM_x sub-modes respectively [26].

Assuming x-directed vector potentials, the transverse fields of the modes at both sides $S = L, R$ can be expressed as follows [25]:

$$\begin{pmatrix} E^S_{\perp x}(x,y) \\ H^S_{\perp x}(x,y) \end{pmatrix} = \sum_{n=n_0}^{N_S} \begin{pmatrix} V^S_n(x) \\ sI^S_n(x) \end{pmatrix} f^S_n(y) \quad S = L, R \tag{1}$$

where V^S_n and I^S_n are the complex amplitudes of the tangential electric and magnetic fields of the sub-mode n, $f^S_n(y)$ is the corresponding tangential field profile and s is a current direction sign. For TE_z: $E_{\perp x} = E_y$, $H_{\perp x} = H_z$, $n_0 = 0$, $s = \pm$ for $S = L, R$ respectively and

$$f^L_n(y) = \sqrt{\frac{\nu_n}{h_L}}\, cos\left(\frac{n\pi}{h_L}y\right),\ f^R_m(y) = \sqrt{\frac{\nu_m}{h_R}}\, cos\left(\frac{m\pi}{h_R}y\right) \tag{2}$$

where $\nu_0 = 1$ and $\nu_{(n,m>0)} = 2$. While for TM_z: $E_{\perp x} = E_z$, $H_{\perp x} = H_y$ and $n_0 = 1$, $s = \mp$ for $S = L, R$ respectively and

$$f^L_n(y) = \sqrt{\frac{2}{h_L}}\, sin\left(\frac{n\pi}{h_L}y\right),\ f^R_m(y) = \sqrt{\frac{2}{h_R}}\, sin\left(\frac{m\pi}{h_R}y\right) \tag{3}$$

As shown in Fig.2(b), the current amplitudes at planes $x = -w_L$ and w_R are defined as I^L_n and I^R_n while at planes $x = 0^-$ and 0^+ as I^{L0}_n and I^{R0}_n. The voltage amplitudes are defined similarly. The current and voltage amplitudes at $x = -w_L$ and w_R are related to those at $x = 0^{\pm}$ by impedance matrices as follows

$$\begin{pmatrix} \underline{V}^L \\ \underline{V}^{L_0} \end{pmatrix} = \mathbf{Z}^L \begin{pmatrix} \underline{I}^L \\ -\underline{I}^{L_0} \end{pmatrix}, \quad \begin{pmatrix} \underline{V}^{R_0} \\ \underline{V}^R \end{pmatrix} = \mathbf{Z}^R \begin{pmatrix} -\underline{I}^{R_0} \\ \underline{I}^R \end{pmatrix} \tag{4}$$

where $\underline{I}^P = \left[I^P_{n_0} ... I^P_{N_S}\right]^\tau$, $\underline{V}^P = \left[V^P_{n_0} ... V^P_{N_S}\right]^\tau$ and $P = \{L, R, L_0, R_0\}$. Also $\mathbf{Z}^S = \begin{pmatrix} \mathbf{Z}^S_{11} & \mathbf{Z}^S_{12} \\ \mathbf{Z}^S_{12} & \mathbf{Z}^S_{11} \end{pmatrix}$ where $\mathbf{Z}^S_{11} = \text{diag}\left\{-jz^S_n cot\left(\kappa^S_n w_S\right)\right\}$, $\mathbf{Z}^S_{12} = \text{diag}\left\{-jz^S_n csc\left(\kappa^S_n w_S\right)\right\}$.

For TM_z case $z^S_n = \eta\frac{\kappa^S_n}{\kappa_0}$ and for TE_z $z^S_n = \eta\frac{\kappa_0}{\kappa^S_n}$, with $\kappa^S_n = \sqrt{\kappa_0^2 - \left(\frac{n\pi}{h_S}\right)^2}$ and $\kappa_0 = \frac{2\pi f}{c_0}$. η and c_0 are the wave impedance and speed in the waveguide medium respectively.

Due to the continuity of the tangential electric and magnetic fields along $x = 0$ plane, a projection matrix $\mathbf{W} = \mathrm{W}_{nm}$ relates the tangential electric and magnetic fields [26] so that:

$$\underline{V}^L = \mathbf{W}\,\underline{V}^R,\ \underline{I}^R = -\mathbf{W}^\tau\,\underline{I}^L,\ \mathrm{W}_{nm} = \int_0^{h_L} f^L_n(y) f^R_m(y) dy \tag{5}$$

$\mathbf{W} = \mathrm{W}_{nm}$, τ for transpose and the minus sign due to the change in the current direction. Finally, the multi-port network shown in Fig.2(b), is represented by the impedance matrix $\mathbf{Z}_T$ that connects the voltages $(\underline{V}^L, \underline{V}^R)$ and currents $(\underline{I}^L, \underline{I}^R)$ at the waveguide ends [26], where $\mathbf{Z}_T =$

$$\begin{pmatrix} \mathbf{Z}^{LL} & \mathbf{Z}^{LR} \\ \mathbf{Z}^{RL} & \mathbf{Z}^{RR} \end{pmatrix} = \begin{pmatrix} \mathbf{Z}^L_{11} - \mathbf{Z}^L_{12}\mathbf{Y}_s\mathbf{Z}^L_{12} & \mathbf{Z}^L_{12}\mathbf{Y}_s\mathbf{W}\mathbf{Z}^R_{12} \\ \mathbf{Z}^R_{12}\mathbf{W}^\tau\mathbf{Y}_s\mathbf{Z}^L_{12} & \mathbf{Z}^R_{11} - \mathbf{Z}^R_{12}\mathbf{W}^\tau\mathbf{Y}_s\mathbf{W}\mathbf{Z}^R_{12} \end{pmatrix}$$

where $\begin{pmatrix} \underline{V}^L \\ \underline{V}^R \end{pmatrix} = \mathbf{Z}_T \begin{pmatrix} \underline{I}^L \\ \underline{I}^R \end{pmatrix}$ and $\mathbf{Y}_s = \left(\mathbf{Z}_{11}^L + \mathbf{W}\mathbf{Z}_{11}^R\mathbf{W}^\tau\right)^{-1}$.

Given $\mathbf{Z}_T$ are known, the cutoff frequencies of the waveguide modes and the corresponding field profiles can be found by applying the PMC boundary conditions at $x = -w_L$ and w_R which correspond to applying open circuit conditions, i.e. $\underline{I}^L = \underline{I}^R = 0$.

b) Cut-off frequency: The cutoff frequencies f_M ($M \in \mathbb{Z}$) of the FSS-GRW can be found following the following steps:

1) Apply the open circuit condition on all right side ports $\underline{I}_2^R = 0$ and all the left side ports except for one port of the sub-mode n.
2) Consider the input admittance of sub-mode n which will be $\left(Z_{nn}^{LL}\right)^{-1}$. The open circuit condition must be also satisfied at the sub-mode n port. Accordingly the sub-mode n resonates (among the resonant mode) at $f = f_M$ if the condition $\left(Z_{nn}^{LL}(f = f_M)\right)^{-1} = 0$ is satisfied, where $I_n^L = \left(Z_{nn}^{LL}\right)^{-1} V_n^L = 0$.
3) By repeating the previous steps over all ports on both sides (L and R); each resonant frequency f_M will be associated with the constituting sets of left and right sub-modes $\{N_{L,M}\}$ and $\{N_{R,M}\}$ respectively.

c) Field Distribution: The field distribution of the $\mathrm{M_{th}}$ waveguide mode is found by examining the matrix $\mathbf{Z}_T$ at the corresponding cutoff frequency $f = f_M$.

1) First by reducing $\mathbf{Z}_T$ into $\mathbf{Z}_{T,M}$ as shown in Fig.2(c). $\mathbf{Z}_{T,M}$ includes only the resonant sub-modes at $f = f_M$ such that

$$\begin{pmatrix} \underline{v}^L \\ \underline{v}^R \end{pmatrix} = \mathbf{Z}_{T,M} \begin{pmatrix} \underline{i}^L \\ \underline{i}^R \end{pmatrix} = \begin{pmatrix} \mathbf{Z}_M^{LL} & \mathbf{Z}_M^{LR} \\ \mathbf{Z}_M^{RL} & \mathbf{Z}_M^{RR} \end{pmatrix} \begin{pmatrix} \underline{i}^L \\ \underline{i}^R \end{pmatrix} \quad (6)$$

where $\mathbf{Z}_M^{RR} = Z_{pq}^{RR}$, $\mathbf{Z}_M^{RL} = Z_{ps}^{RL}$, $\mathbf{Z}_M^{LR} = Z_{rq}^{LR}$, $\mathbf{Z}_M^{LL} = Z_{rs}^{LL}$ with $\underline{v}^L = v_t^L = V_p^L$, $\underline{i}^L = i_t^L = I_q^L$, $\underline{v}^R = v_u^R = V_r^R$, $\underline{i}^R = i_u^R = I_s^R$, where $r, s \in \{N_{L,M}\}$ and $p, q \in \{N_{R,M}\}$. Note the change in indexing where $t = \{1, ..., \text{size}(\{N_{L,M}\})\}$ and $u = \{1, ..., \text{size}(\{N_{R,M}\})\}$.
2) The sub-matrices $\left(\mathbf{Z}_M^{RR}\right)^{-1}$, $\left(\mathbf{Z}_M^{LL}\right)^{-1}$ are singular matrices, this can be shown as follows

$$\because \underline{i}^R = 0, \ \therefore \underline{i}^L = \left(\mathbf{Z}_M^{LL}\right)^{-1} \underline{v}^L = 0 \cdot \underline{e}^L$$
$$\because \underline{i}_1^L = 0, \ \therefore \underline{i}^R = \left(\mathbf{Z}_M^{RR}\right)^{-1} \underline{v}^R = 0 \cdot \underline{e}^R$$

where $\underline{e}^L$ and $\underline{e}^R$ are the unit colmon vectors ($\left[\underline{e}^S\right]^\tau \cdot \underline{e}^S = 1$) and they are the eigenvectors of the matrices $[Z_{LL}]^{-1}$ and $[Z_{RR}]^{-1}$ respectively with zero eigenvalues. The vectors $\underline{e}^S$ determine the relative amplitude ratios of waveguide sub-modes on the same side S. In general, at resonance, the four sub-matrices are singular value decomposed into

$$\mathbf{Z}_M^{SS'} = z_M^{SS'} \ \underline{e}^S \left[\underline{e}^{S'}\right]^\tau \text{ with } \lim_{f \to f_M} z_M^{SS'} = \infty \quad (7)$$

where $S, S' = \{L, R\}$. Accordingly, $\underline{e}^S$ are extracted directly from the columns and rows of the $\mathbf{Z}_M$.

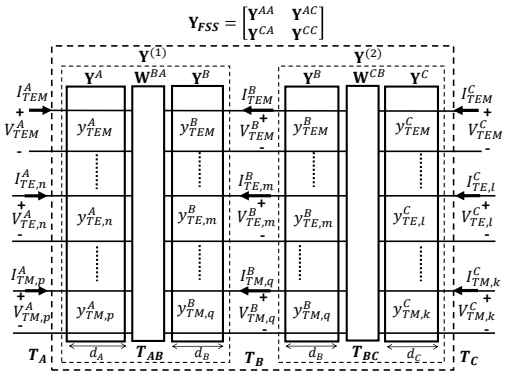

Fig. 3. Multi-port network representation in terms of the full FSS admittance matrix $\mathbf{Y}_{FSS}$ which is found by cascading $\mathbf{Y}^{(1)}$ (between T_A and T_B) and $\mathbf{Y}^{(2)}$ (between T_B and T_C). n, m, p, q and $k \in \mathbb{Z}$ are the ports indices.

3) The relative value between the sub-modes amplitudes on both sides is found as follows: $\because \underline{i}^R = 0$ and $\because \underline{i}^L = 0$

$$\therefore \underline{v}^R = \lim_{f \to f_M} \mathbf{Z}_M^{RL} \left[\mathbf{Z}_M^{LL}\right]^{-1} \underline{v}^L = \gamma_M \ \underline{e}^R \left[\underline{e}^L\right]^\tau \underline{v}^L$$

$$\therefore \underline{v}^L = \lim_{f \to f_M} \mathbf{Z}_M^{LR} \left[\mathbf{Z}_M^{RR}\right]^{-1} \underline{e}^R = \frac{1}{\gamma_M} \ \underline{e}^L \left[\underline{e}^R\right]^\tau \underline{v}^R$$

where $\gamma_M = \lim_{f \to f_M} \frac{z_M^{RL}}{z_M^{LL}} = \lim_{f \to f_M} \frac{z_M^{RR}}{z_M^{LR}} < \infty$.
4) By letting $\underline{v}^L = \underline{e}^L$ and $\underline{v}^R = \gamma_M \underline{e}^R$, then $V_r^L = e_t^L$ and $V_p^R = \gamma_M e_u^R$ using the same indices as in eq.(3). Finally, the amplitudes of the z-component fields in eq.(1) are found using ABCD matrix [25].

For the M^{th} TM_z waveguide mode aperture field distribution can be written as follows:

$$E_{z,M}(x,y) = \frac{1}{\Lambda_M} \Bigg[u(-x) \sum_{r \in \{N_{L,M}\}} V_r^L cos(\kappa_r^L (x + w_L)) \ sin(\frac{r\pi}{h_L} y) + u(x) \sum_{p \in \{N_{R,M}\}} V_p^R cos(\kappa_p^R (x - w_R)) sin(\frac{p\pi}{h_R} y) \Bigg] \quad (8)$$

where $u(x) = 1$ for $x > 0$ and $u(x) = 0$ for $x < 0$. $\Lambda_M = \sqrt{\int_0^{h_R} \int_{-w_L}^{w_R} |E_{\perp z,M}(x,y)|^2 dx dy}$ is to normalize the field. The transverse field components are found $E_{\perp z,M} = -j \frac{\kappa_{z,M}}{\kappa_{c,M}^2} \nabla_{\perp z} E_{z,M}(x,y)$, where $\kappa_{c,M} = \frac{2\pi f_M}{c_0}$, $\kappa_{z,M} = \sqrt{\kappa_0^2 - \kappa_{c,M}^2}$ and $\nabla_{\perp z} = \hat{x}\partial_x + \hat{y}\partial_y$. On the other hand, the M^{th} TE_z transverse field components are found as follows: $E_{\perp z,M} = j \frac{\kappa_0 \eta}{\kappa_{c,M}^2} (\hat{z} \times \nabla_{\perp z} H_{z,M}(x,y))$, where

$$H_{z,M}(x,y) = \frac{j}{\Lambda_M} \Bigg[u(-x) \sum_{r \in \{N_{L,M}\}} \frac{V_r^L}{z_r^L} sin(\kappa_r^L (x + w_L)) \ cos(\frac{r\pi}{h_L} y) - u(x) \sum_{p \in \{N_{R,M}\}} \frac{V_p^R}{z_p^R} sin(\kappa_p^R (x - w_R)) cos(\frac{p\pi}{h_R} y) \Bigg] \quad (9)$$

III. Generalized Network Formulation

In this section, we summarize the computational steps of the multi-modal admittance matrix $Y^{(1)}$ of the GRW A connected

to the FSS-GRW B through the interface T_{AB} as shown in Fig. 3. The admittance matrix $Y^{(2)}$due to the interface between GRWs B and C can be found similarly and the full admittance matrix $\mathbf{Y}_{FSS} = \begin{pmatrix} \mathbf{Y}^{AA} & \mathbf{Y}^{AC} \\ \mathbf{Y}^{CA} & \mathbf{Y}^{CC} \end{pmatrix}$ between the reference planes T_A and T_C is found by cascading $Y^{(1)}$ and $Y^{(2)}$ networks. The reader is referred to [26] for a detailed treatment of the generalized network formalism. As shown in Fig. 3, at the reference planes T_S ($S = A, B$), every port P of the network corresponds to a GRW mode where $P = \{\text{TEM, TM}_m, \text{or TE}_n\}$ $(n, m \geq 1)$. The voltages and currents at the ports of each waveguide are the amplitudes of the vector tangential electric $\bar{E}^S_{\perp z,P}(x,y)$ and magnetic $\bar{H}^S_{\perp z,P}(x,y)$ fields. These current and voltages are related by the admittance matrix $\mathbf{Y}^{(1)}$ whose submatrices are computed as follows: $\mathbf{Y}^{(1)} = \begin{pmatrix} \mathbf{Y}^A_{11} - \mathbf{Y}^A_{12}\mathbf{W}^{BA}\mathbf{Z}_s[\mathbf{W}^{BA}]^\tau\mathbf{Y}^A_{12} & -\mathbf{Y}^A_{12}\mathbf{W}^{BA}\mathbf{Z}_s\mathbf{Y}^B_{12} \\ -\mathbf{Y}^B_{12}\mathbf{Z}_s[\mathbf{W}^{BA}]^\tau\mathbf{Y}^A_{12} & \mathbf{Y}^B_{11} - \mathbf{Y}^B_{12}\mathbf{Z}_s\mathbf{Y}^B_{12} \end{pmatrix}$ where $\mathbf{Z}_s = \left(\mathbf{Y}^B_{11} - \left[\mathbf{W}^{BA}\right]^\tau \mathbf{Y}^A_{11}\mathbf{W}^{BA}\right)^{-1}$. The elements of the two sub-matrices are defined such that: $\mathbf{Y}^S_{11} = [Y^S_{11}]_{PP} = -j\,\text{diag}\left\{y^S_P cot\left(\kappa^S_P d_S\right)\right\}$, $\mathbf{Y}^S_{12} = [Y^S_{12}]_{PP} = -j\,\text{diag}\left\{y^S_P csc\left(\kappa^S_P d_S\right)\right\}$. y^S_P and κ^S_P are the modal wave impedance and propagation constant respectively. The projection matrix $\mathbf{W}^{BA} = W^{BA}_{QP}$ relates the transverse (to the z-axis) electric and magnetic field components of the waveguides A and B at the interface T_{AB}. The elements of the transition matrix [27], [28] are defined as follows with $P, Q = \{\text{TEM, TM}_m, \text{or TE}_n\}$ $(n, m \geq 1)$:

$$W^{BA}_{QP} = \int_{T_{AB}} \bar{E}^B_{\perp z,Q}(x,y) \cdot \bar{E}^A_{\perp z,P}(x,y)dxdy \qquad (10)$$

IV. Numerical Validation

The proposed procedure was validated by the full-wave simulations using Ansys HFSS. Computations are done using the dimensions $d_A = d_C = 0.1$mm, $d_B = 0.5$mm, $d_x = 1.57$mm, $d_y = 7.1$mm, $P_x = 8.13$mm, and $P_y = 10.2$mm and all media are assumed to be of vacuum. To achieve convergence for all polarizations, the number of sub-modes in GRW B depends on the ratios $\frac{N_L}{N_R} \sim \frac{h_L}{h_R}$ [29], with $N_R = 150$ was chosen. Fig. 4(a) shows the first three elements of $\mathbf{Y}^{AA}$ and $\mathbf{Y}^{AC}$ respectively. The plots show agreement over a large frequency range even beyond the cutoff frequency of the first high-order resonance in GRW B (26.66 GHz).

In the frequency range where waveguides A and C are mono-modal, below the 1st higher order cutoff frequency $f \leq 29.36$ GHz; a lumped circuit model [19] can be extracted by choosing the planes T_A and T_C far enough from the FSS so that higher order modes are confined near the FSS. In this case, the multi-port network (Fig. 3) reduces to a two-port network (Fig. 4(b)) by closing the ports of the higher modes on their corresponding wave admittances. After deembedding [25], the FSS is modeled as a pi-network with series and parallel admittances respectively Y_s and Y_p. Furthermore, the pi-network can be approximated by lumped components with validity around the frequency of interest as shown in Fig.4.b. Around 10 GHz, Y_s and Y_p are approximated by $C_s = 79.1$ fF, $L_s = 0.73$ nH, $C_p = 16.2$ fF and $L_s = 3.54$ nH at

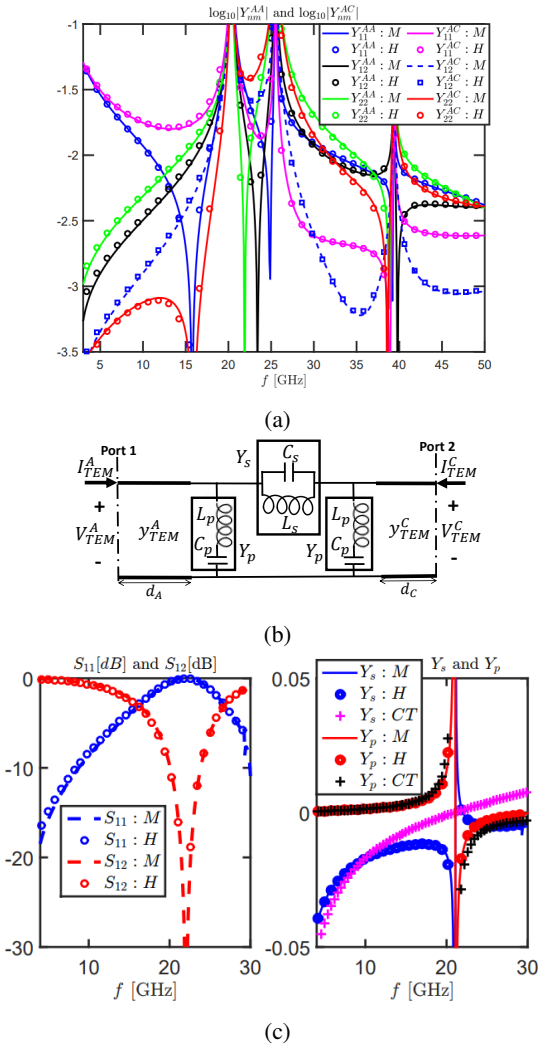

Fig. 4. (a) The first three elements of Y-matrices $\mathbf{Y}^{AA}$ and $\mathbf{Y}^{AC}$ in logarithmic scale with $d_A = d_C = 0.1$mm. Note $\mathbf{Y}^{AA} = \mathbf{Y}^{CC}$ and $\mathbf{Y}^{AC} = \mathbf{Y}^{CA}$. (b) Reduced two-port network as seen by the propagating TEM modes at the A and C ports. (c) Scattering parameters of the reduced two-port network ($d_A = d_C = 10$mm) and the admittances of the pi-network representation of the FSS (Y_s and Y_p). M stands for this method, H for HFSS and CT is for the lumped circuit approximation at 10 GHz.

10 GHz. Fig. 4(c) shows agreement between the computed scattering parameters and the pi-network admittances of the reduced two-port network with the full-wave simulations, also it shows agreement with the lumped circuit around 10 GHz.

V. Conclusion

A generalized transverse resonance method was proposed to compute analytically the aperture field of a Frequency Selective Surface (FSS) unit cell with arbitrary thickness upon normal incidence. This approach allows the extraction of a multi-modal equivalent network as well as single-moded lumped circuits of the FSS specific for incident field polarization. The proposed method was verified numerically versus full-wave simulation using a patch-based FSS as a case study. The proposed model is valid beyond the excitation frequencies of the FSS aperture higher modes and for closely packed cascaded FSS as well.

REFERENCES

[1] B. Munk, Ed. *Frequency Selective Surfaces: Theory and Design*, New York: Wiley, 2000.

[2] M.-A. Joyal and J.-J. Laurin, "Analysis and Design of Thin Circular Polarizers Based on Meander Lines," *IEEE Trans. Antennas Propag.*, vol. 60, no. 6, pp. 3007-3011, June 2012.

[3] J. E. Varela and J. Esteban, "Characterization of waveguides with a combination of conductor and periodic boundary contours: Application to the analysis of bi-periodic structures," *IEEE Trans. Microw. Theory Tech.*, vol. 60, no. 3, pp. 419–430, Mar. 2012.

[4] F. Mesa, R. Rodriguez-Berral and F. Medina, "Unlocking Complexity Using the ECA: The Equivalent Circuit Model as An Efficient and Physically Insightful Tool for Microwave Engineering," *IEEE Microw. Mag.*, vol. 19, no. 4, pp. 44-65, June 2018.

[5] E. Baladi and S. V. Hum, "Equivalent circuit models for metasurfaces using Floquet modal expansion of surface current distributions,"*IEEE Trans. Antennas Propag.*, vol. 69, pp. 5691–5703, 2021.

[6] A. Alex-Amor, F. Mesa, Á. Palomares-Caballero, C. Molero and P. Padilla, "Exploring the Potential of the Multi-Modal Equivalent Circuit Approach for Stacks of 2-D Aperture Arrays," *IEEE Trans. Antennas Propag.*, vol. 69, no. 10, pp. 6453-6467, Oct. 2021.

[7] C. Molero, R. Rodríguez-Berral, F. Mesa and F. Medina, "Analytical Circuit Model for 1-D Periodic T-Shaped Corrugated Surfaces," *IEEE Trans. Antennas Propag.*, vol. 62, no. 2, pp. 794-803, Feb. 2014.

[8] R. Rodríguez-Berral, C. Molero, F. Medina, and F. Mesa, "Analytical wideband model for strip/slit gratings loaded with dielectric slabs," *IEEE Trans. on Microw. Theory Techn.*, vol. 60, no. 12, pp. 3908–3918, Dec. 2012.

[9] F. Mesa, R. Rodríguez-Berral, and F. Medina, "On the limitations of equivalent circuits for the modeling of periodic structures," in *Proc. IEEE MTT-S Int. Microw. Workshop Ser. Adv. Mater. Processes RF THz Appl. (IMWS-AMP)*, Pavia, Italy, Sep. 2017, pp. 1–3.

[10] A. Barlabe, A. Comeron and L. Pradell, "Generalized transverse resonance analysis of planar discontinuities considering the edge effect," *IEEE Microwave Guided Wave Lett.*, vol. 10, no. 12, pp. 517-519, Dec. 2000.

[11] R. Sorrentino, "Transverse resonance technique," in *Numerical Techniques for Microwave and Millimeter-Wave Passive Structures*, T. Itoh, Ed. New York: Wiley, 1989, ch.11.

[12] F. Medina, R. Rodríguez-Berral and F. Mesa, "Circuit model for metallic gratings with tapered and stepped slits," *2012 42nd European Microwave Conference*, Amsterdam, Netherlands, 2012, pp. 1225-1228.

[13] B. Bates and G. Staines, "Transverse Resonance Analysis Technique for Microwave and Millimetre-Wave Circuits". Defence Science and Technology Organization Canberra (Australia); 1994 Feb 1.

[14] R. Sorrentino and T. Itoh, "Transverse resonance analysis of finline discontinuities," *IEEE Trans. Microwave Theoy Tech.*, vol. MTT-32, pp. 1633-1638, Dec. 1984.

[15] J. P. Montgomery, "On the Complete Eigenvalue Solution of Ridged Waveguide," *IEEE Trans. on Microw. Theory Techn.*, vol. 19, no. 6, pp. 547-555, Jun. 1971.

[16] V. Labay and J. Bornemann, "Matrix singular value decomposition for pole-free solutions of homogeneous matrix equations as applied to numerical modeling methods," *IEEE Microwave Guided Wave Lett.*, vol. 2, no. 2, pp. 49-51, Feb. 1992.

[17] G. Schiavon, R. Sorrentino, and P. Tognolatti, "Characterization of coupled finlines by generalized transverse resonance method," *Int. J. Numerical Modeling: Electron. Networks, Devices and Fields*, vol.1. pp.45-59, Mar.1988.

[18] F. Alessandri, G. Bartolucci, and R. Sorrentino, "Admittance matrix formulation of waveguide discontinuity problems: Computer-aided design of branch guide couplers," *IEEE Trans. Microwave Theory Tech.*, vol.36, pp. 394–403, Feb. 1988

[19] F. Costa, A. Monorchio, and G. Manara, "Efficient analysis of frequency-selective surfaces by a simple equivalent-circuit model," IEEE Antennas Propag. Mag., vol. 54, no. 4, pp. 35–48, Aug. 2012.

[20] O. Luukkonen et al., "Simple and Accurate Analytical Model of Planar Grids and High-Impedance Surfaces Comprising Metal Strips or Patches," *IEEE Trans. Antennas Propag.*, vol. 56, no. 6, pp. 1624-1632, June 2008.

[21] T. Zhao, D. R. Jackson, J. T. Williams, H.-Y. D. Yang, and A. A. Oliner, "2-D periodic leaky-wave antennas-Part I: Metal patch design," *IEEE Trans. Antennas Propag.*, vol. 53, no. 11, pp. 3505–3514, Nov. 2005.

[22] S. Tretyakov, Analytical Modeling in Applied Electromagnetics, Norwood, MA, Artech House, 2003.

[23] S. Monni, G. Gerini, A. Neto, and A. Tijhuis, "Multimode Equivalent Networks for the Design and Analysis of Frequency Selective Surfaces," *IEEE Trans. Antennas Propag.*, AP-55, 10, October 2007, pp.2824-2835.

[24] F. Medina, F. Mesa and R. Marques, "Extraordinary Transmission Through Arrays of Electrically Small Holes From a Circuit Theory Perspective," *IEEE Trans. on Microw. Theory Techn.*, vol. 56, no. 12, pp. 3108-3120, Dec. 2008.

[25] D. Pozar, *Microwave engineering*, New York: Wiley, 2011.

[26] M. Guglielmi, R. Sorrentino, and G. Conciauro, Eds., *Advanced Modal Analysis: CAD Techniques for Waveguide Components and Filter*, New York: Wiley, 1991.

[27] P. Guillot, P. Couffignal, H. Baudrand and B. Theron, "Improvement in calculation of some surface integrals: application to junction characterization in cavity filter design," *IEEE Trans. Microwave Theory Tech.*, vol. 41, no. 12, pp. 2156-2160, Dec. 1993.

[28] G. Figlia and G. G. Gentili, "On the line-integral formulation of mode matching technique," *IEEE Trans. Microw. Theory Tech.*, vol. 50, no. 2, pp. 578–580, Feb. 2002.

[29] M. Leroy, "On the convergence of numerical results in modal analysis," *IEEE Trans. Antennas Propag.*, vol. 31, no. 4, pp. 655-659, July 1983.